












Received: 30 May 2023

Revised: 9 September 2023

Accepted: 10 September 2023

# Sensitive and high laser damage threshold substrates for surface-enhanced Raman scattering based on gold and silver nanoparticles

Felix Mayr<sup>1</sup>  | Robert Zimmerleiter<sup>2</sup>  | Patricia M. A. Farias<sup>3</sup> | Mateusz Bednorz<sup>1</sup>  |  
Yolanda Salinas<sup>4</sup>  | André Galemek<sup>5</sup>  | Olavo D. F. Cardozo<sup>6</sup> |  
Dominik Wielend<sup>1</sup>  | Dyego Oliveira<sup>7</sup> | Raquel Milani<sup>7</sup> | Tania M. Brito-Silva<sup>8</sup>  |  
Markus Brandstetter<sup>2</sup> | Eduardo Padrón-Hernández<sup>7</sup>  | Peter Burgholzer<sup>2</sup>  |  
Andreas Stingl<sup>6</sup> | Markus C. Scharber<sup>1</sup>  | Niyazi Serdar Sariciftci<sup>1</sup> 

<sup>1</sup>Linz Institute for Organic Solar Cells (LIOS), Institute of Physical Chemistry, Johannes Kepler University Linz, Linz, Austria

<sup>2</sup>RECENDT – Research Center for Non-Destructive Testing GmbH, Linz, Austria

<sup>3</sup>Departamento de Biofísica e Radiobiologia, Federal University of Pernambuco, Cidade Universitaria, Recife, Brazil

<sup>4</sup>Institute of Polymer Chemistry (ICP), Johannes Kepler University Linz, Linz, Austria

<sup>5</sup>Departamento de Química Fundamental, Federal University of Pernambuco, Recife, Brazil

<sup>6</sup>Phornano Holding GmbH, Korneuburg, Austria

<sup>7</sup>Departamento de Física, Federal University of Pernambuco, Recife, Brazil

<sup>8</sup>Departamento de Ciências Exatas, Santa Cruz State University, Ilheus, Brazil

## Correspondence

Felix Mayr, Linz Institute for Organic Solar Cells (LIOS), Institute of Physical Chemistry, Johannes Kepler University Linz, Altenberger Straße 69, 4040 Linz, Austria.  
Email: [felix.mayr@jku.at](mailto:felix.mayr@jku.at)

## Funding information

Austrian Research Promotion Agency (FFG), Grant/Award Numbers: 874147, 888408; Johannes Kepler Open Access Publishing Fund of the Johannes Kepler University Linz

## Abstract

Surface-enhanced Raman scattering (SERS) is a sensitive and fast technique for sensing applications such as chemical trace analysis. However, a successful, high-throughput practical implementation necessitates the availability of simple-to-use and economical SERS substrates. In this work, we present a robust, reproducible, flexible and yet cost-effective SERS substrate suited for the sensitive detection of analytes at near-infrared (NIR) excitation wavelengths. The fabrication is based on a simple dropcast deposition of silver or gold nanomaterials on an aluminium foil support, making the design suitable for mass production. The fabricated SERS substrates can withstand very high average Raman laser power of up to 400 mW in the NIR wavelength range while maintaining a linear signal response of the analyte. This enables a combined high signal enhancement potential provided by (i) the field enhancement via the localized surface plasmon resonance introduced by the noble metal nanomaterials and (ii) additional enhancement proportional to an increase of the applicable Raman laser power without causing the thermal decomposition of the analyte. The application of the SERS substrates for the

**Abbreviations:** AEF, Analytical enhancement factor; LOD, limit of detection; LSPR, localized surface plasmon resonance; NIR, near-infrared; NP, nanoparticle; NPL, nanoplate; ppm, parts per million; ppb, parts per billion; R6G, rhodamine 6G; SEM, scanning electron microscopy; SERS, surface-enhanced Raman scattering; TEM, transmission electron microscopy.

This is an open access article under the terms of the [Creative Commons Attribution-NonCommercial](https://creativecommons.org/licenses/by-nc/4.0/) License, which permits use, distribution and reproduction in any medium, provided the original work is properly cited and is not used for commercial purposes.

© 2023 The Authors. *Analytical Science Advances* published by Wiley-VCH GmbH.

trace detection of melamine and rhodamine 6G is demonstrated, which shows limits of detection smaller than 0.1 ppm and analytical enhancement factors on the order of  $10^4$  as compared to bare aluminium foil.

**KEYWORDS**

gold nanoparticles, melamine, silver nanoplates, surface-enhanced Raman scattering, trace chemical detection

## 1 | INTRODUCTION

The incidence of light on a continuous metallic surface may give rise to distinct phenomena, such as the photoelectric effect<sup>1,2</sup> and the excitation of collective free electron oscillations at the metal surface (surface plasmons).<sup>3,4</sup> When the metallic surface is structured in nanometric dimensions smaller than the wavelength of incident light, the spatially confined resonant collective electron oscillations lead to an enhancement of the local electromagnetic field, generating a localized surface plasmon resonance (LSPR).<sup>4-6</sup> Surface-enhanced Raman scattering (SERS) takes place when the enhancement of the localized electromagnetic field results in the augmentation of the Raman scattering cross-section of molecules located in the vicinity (several nanometres) of the nanostructured metallic surface.<sup>7-9</sup> Enhancements of the resulting Raman signal intensities in the order of up to  $\sim 10^{12}$  under ideal conditions have been reported, which allow the detection of single molecules.<sup>10</sup> These potentially large signal enhancements make SERS a very powerful technique in sensing applications for the sensitive, fast and cost-efficient trace detection of chemicals, such as explosives,<sup>11-13</sup> pesticides,<sup>14-16</sup> pharmaceuticals,<sup>17,18</sup> biomolecules<sup>19-21</sup> and food contaminants.<sup>22-24</sup> Among these applications, the sensitive detection of trace pollutants and contaminants in foods and feedstuffs by SERS are especially important tasks to prevent negative effects of these chemicals on the health of humans and animals.

Most commonly used SERS platforms are based on nanostructural metallic surfaces, primarily of the metals Au, Ag or Cu.<sup>22,25</sup> These can comprise metal nanomaterials in colloidal dispersion or immobilized on solid substrates, as well as nanostructured metal films.<sup>22</sup> The wavelength range of the LSPR absorption bands of the employed nanomaterials and, thus, the suitable excitation wavelengths for SERS depend on the type of used metal, size and shape of the nanomaterial, interparticle distance and the surrounding medium.<sup>26-29</sup> SERS measurements are typically conducted at excitation wavelengths between 400 and 800 nm; however, the application of near-infrared (NIR) excitation wavelengths, for example 1064 nm, is gaining increasing importance.<sup>25,30-33</sup> The advantages of NIR excitation are the avoidance of interference from fluorescence, the reduction of photobleaching and decreased analyte heating for many organic molecules due to the absence of NIR light absorption,<sup>25,31,32</sup> providing ideal conditions for the measurement of sensitive analytes such as biomolecules.<sup>33</sup> To achieve NIR-SERS, various types of nanomaterials have been

employed, including bimetallic Au/Ag nanostars,<sup>25</sup> Au films evaporated onto silica nanospheres,<sup>31</sup> Ag-coated porous silicon<sup>32</sup> poly-disperse Au colloids,<sup>34</sup> aggregated colloidal Ag nanoparticles (NPs)<sup>31,35,36</sup> Au nanorods<sup>37</sup> and hollow Au nanoshells.<sup>38</sup>

For a fast and straightforward in-field application of SERS sensors, the development of ready-to-use SERS substrates is crucial. Besides the type of plasmonic nanomaterial, the choice of support material onto which the SERS-active metallic nanostructures are deposited is an essential parameter for achieving a high sensitivity, reproducibility and robustness of the SERS platforms. Commonly used support materials for the fabrication of SERS substrates include paper, polymers, glass or silicon.<sup>39</sup> Aluminium is another solid support material with favourable properties for fabricating SERS substrates, such as low cost, high reflectivity,<sup>40</sup> absence of a substrate Raman signal or fluorescence<sup>41</sup> and large thermal conductivity for fast heat dissipation.<sup>42</sup> Furthermore, nanostructured Al shows plasmon resonances that are tuneable from the UV to the NIR wavelength range and exhibits a pronounced SERS effect.<sup>43,44</sup> Gudun et al. found a signal enhancement even for untreated commercial Al foil and reported analytical enhancement factors (AEFs) of 80–240 for bare Al foil at excitation wavelengths of 633 and 785 nm, respectively.<sup>40</sup> A synergistic enhancement can thus be obtained when combining plasmonic metal nanomaterials with aluminium support materials for SERS substrates. Gudun and co-workers reported AEFs of about  $10^7$  for the detection of 4-nitrobenzenethiol and crystal violet and a limit of detection (LOD) for melamine of 27 ppb at 785 nm excitation on SERS substrates of AuNPs on Al foil.<sup>40</sup> Martinez-Garcia et al. reported an AEF of ca.  $10^7$  for the detection of rhodamine 6G (R6G) (at  $10^{-13}$  M) on SERS substrates of concave Au nanocubes deposited onto 3-aminopropyltriethoxysilane (APTS)-treated aluminium (Al-6063) slides.<sup>41</sup> Ceballos et al. used electrodeposited Ag nanodendrites on aluminium as SERS substrates and reported enhancement factors of up to  $4 \times 10^4$  for R6G detection.<sup>45</sup>

In this work, we report the fabrication of SERS substrates with extraordinarily high acceptable laser excitation power and high analyte sensitivities at NIR excitation wavelengths (785 and 1064 nm) based on a cost-effective and very simple dropcast deposition of Ag nanoplates or spherical Au nanoparticles on untreated aluminium foil. The fabricated substrates are compared to commercial substrates based on a similar fabrication method. We demonstrate the application of the SERS substrates for the sensitive detection of melamine and R6G at concentrations of 0.1 ppm and below. This is of high relevance for quality control of food and drinking water, due to the harmfulness of

melamine and its abuse as an adulterant in milk and infant formula in the past, which led to a very high number of hospitalizations and even fatalities among infants.<sup>46</sup>

## 2 | EXPERIMENTAL SECTION

### 2.1 | Materials and instruments

Silver nitrate ( $\text{AgNO}_3$ , 99%), melamine (>99%), trisodium citrate dihydrate (99%), poly(ethylene glycol) (average  $M_n = 3350 \text{ g mol}^{-1}$ , 99%) and sodium borohydride ( $\text{NaBH}_4$ ,  $\geq 98\%$ ) were obtained from Sigma-Aldrich. R6G ( $\geq 99\%$ ) was obtained from TCI Chemicals. Ethanol (p.a.) and hydrogen peroxide (30% (w/w) in water) were obtained from VWR. Ultrapure water was obtained from a Sartorius Arium Mini water purification system. Aluminium foil (Rotilabo) was obtained from Carl Roth.

UV-Vis-NIR absorption spectra were recorded on a PerkinElmer Lambda1050 spectrophotometer. Raman spectroscopy at an excitation wavelength of 1064 nm was performed on a Bruker MultiRAM FT-Raman spectrometer using a liquid nitrogen-cooled Ge detector. Measurements at 1064 nm excitation wavelength on samples in powder form were conducted on a Bruker RamanScope III Raman microscope coupled to the FT-Raman spectrometer. The excitation laser spot diameter was ca. 50  $\mu\text{m}$ . Measurements at 1064 nm were performed with a resolution of  $4 \text{ cm}^{-1}$  and by averaging 100 scans. Raman spectroscopy at an excitation wavelength of 785 nm was performed on a Wasatch Photonics WP Raman spectrometer equipped with a fibre-coupled Raman probe providing laser excitation with a spot size of ca. 160  $\mu\text{m}$  and a resolution of  $9 \text{ cm}^{-1}$ . Spectra were recorded with an integration time of 1 s and an average of 10 scans.

Scanning electron microscopy (SEM) was performed on a ZEISS Cross Beam XB 1540 scanning electron microscope. An acceleration voltage of 3 kV and a working distance of 3.6 mm were used. Optical microscopy was performed on a Nikon Eclipse LV100ND.

Samples for transmission electron microscopy (TEM) analysis were prepared by dropcasting a dilute aqueous sample dispersion onto holey-carbon TEM 300 Mesh copper grids. Detailed structural characterization was obtained using a JEOL JEM-2200FS TEM operated at 200 kV. The size distributions were evaluated by the analysis of TEM micrographs using ImageJ software (National Institute of Health) for more than 350 particles. Particle size histograms were fitted with a Gaussian distribution function.

### 2.2 | Nanomaterials for SERS substrates

Silver nanoplates (AgNPLs) were prepared by a procedure adapted from the method reported by Zhang et al.<sup>47</sup> Under ambient conditions, 40  $\mu\text{L}$  of a 50 mM  $\text{AgNO}_3$  solution, 400  $\mu\text{L}$  of a 75 mM trisodium citrate dihydrate solution, 40  $\mu\text{L}$  of a 17.5 mM poly(ethyleneglycol) (average  $M_n = 3350$ ) solution and 48  $\mu\text{L}$  concentrated  $\text{H}_2\text{O}_2$  solution (30% w/w) were added to 20 mL of ultrapure water. To this solution, 120  $\mu\text{L}$  of a

100 mM  $\text{NaBH}_4$  solution was swiftly added under vigorous stirring to yield a faintly yellow solution. The solution was stirred for 30 min at room temperature during which its colour changed from yellow via red to dark blue. The resulting dark blue AgNPL dispersion was stored at  $4^\circ\text{C}$  for 12 h. The dispersion was centrifuged at 5000 rpm for 90 min, and the precipitate was washed with ultrapure water. The centrifugation and washing were carried out twice. The final precipitate was redispersed in 1 mL of ultrapure water to yield a concentrated AgNPL dispersion used for the fabrication of SERS substrates.

Gold nanoparticle dispersions (HiQuant AUHQ40,  $>0.8 \text{ mg mL}^{-1}$ ) were obtained from Phornano and used as received.

### 2.3 | SERS substrate fabrication

For SERS substrate fabrication, aluminium foil was cleaned by ultrasonication in acetone for 15 min, followed by thorough washing with ultrapure water and blow-drying with pressurized nitrogen gas. The cleaned Al foil was attached to a glass slide with double-sided adhesive tape for easier handling and to provide a flat sample surface. Drop-cast deposition was carried out by depositing 50  $\mu\text{L}$  of the AgNPL or AuNP dispersion on the Al foil, and the substrate was left to dry at room temperature under ambient atmosphere. After drying, the deposition step was carried out a second time resulting in a total volume of 100  $\mu\text{L}$  of nanoparticle dispersion used per substrate. For comparison with the fabricated SERS substrates, commercially available SERS substrates (Phornano 4n4SERS) based on gold nanoparticles on Al foil were used.

### 2.4 | SERS substrate application for analyte detection

Melamine and R6G were used as target analytes for the test of the fabricated SERS substrates. Stock solutions of melamine and R6G in ultrapure water (1000 ppm) were prepared and diluted with the respective solvent to achieve the desired concentrations. Analyte solutions of 10  $\mu\text{L}$  were dropcast-deposited onto the active area of the SERS substrate and dried at room temperature under ambient conditions before performing Raman spectroscopy measurements.

The AEFs were estimated for the SERS substrates according to Equation (1).<sup>10,44</sup> Here,  $I_{\text{SERS}}$  and  $I_{\text{RS}}$  are the Raman signal intensities under SERS conditions and without surface enhancement, respectively, whereas  $c_{\text{SERS}}$  and  $c_{\text{RS}}$  represent the analyte solution concentrations used for the measurements with and without SERS, respectively. In our study, we used the peak areas of the measured Raman peaks as values for  $I_{\text{SERS}}$  and  $I_{\text{RS}}$ :

$$\text{AEF} = \frac{I_{\text{SERS}}/c_{\text{SERS}}}{I_{\text{RS}}/c_{\text{RS}}} \quad (1)$$

The LODs of the investigated SERS substrates were determined from the minimum peak area limit required for analyte detection,  $I_{\text{LOD}}$ . The peak area limit was calculated from the mean peak area measured

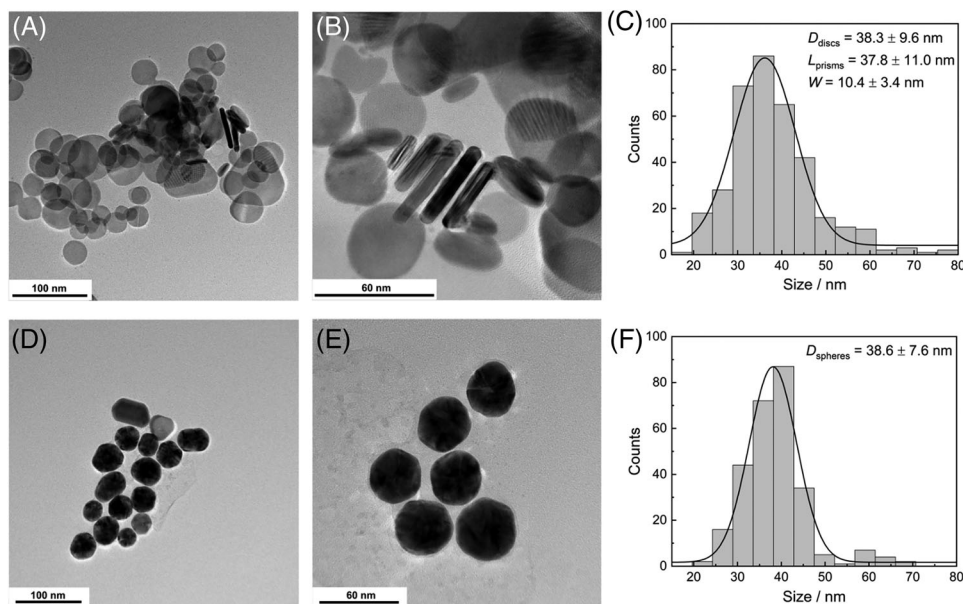


**FIGURE 1** (A) Transmission electron microscopy (TEM) images of the synthesized silver nanocrystals showing the different shapes of the silver nanoplates. (B) Silver nanoplates arranged in a face-to-face aligned stack. (C) Histogram of the size distribution fitted with a Gaussian distribution function as determined from 350 nanodiscs. Inset gives the mean diameter of nanodiscs, the mean length of nanoprisms and mean width of the nanocrystals (average length and width of the vertically located nanoplates were calculated from 100 nanoparticles, analysed from TEM micrographs). (D and E) TEM images of the used gold nanoparticles at different scales. (F) Histogram of the size distribution of spherical Au nanoparticles fitted with a Gaussian distribution function determined from 270 nanoparticles. The inset gives the average sphere diameter.

for blank SERS substrates without analyte,  $\bar{I}_{\text{Blank}}$ , and the standard deviation of the peak areas measured for the blank replicates,  $s_{\text{Blank}}$ , according to the following equation<sup>44</sup>:

$$I_{\text{LOD}} = \bar{I}_{\text{Blank}} + 3 \cdot s_{\text{Blank}} \quad (2)$$

From the peak area limit  $I_{\text{LOD}}$ , the corresponding LOD in terms of analyte concentration was calculated from the linear fit function determined from the measurements of different analyte concentrations on the respective SERS substrates.

### 3 | RESULTS AND DISCUSSION

#### 3.1 | Nanoparticle characterization

The morphological shapes and size distribution of the used Ag nanoplates and Au nanoparticles were investigated by TEM. TEM micrographs (Figure 1A) revealed the occurrence of nanocrystals of different shapes in the synthesized AgNPL samples. Mainly disc-shaped silver nanoplates were observed, whereas also a minority of truncated prism-shaped nanoplates were present. The planar and triangular shape nanoprisms tended to stand face-to-face together, vertically upon their edges, which appear like rod-shaped nanoparticles (see Figure 1B), an effect well known and previously reported.<sup>16,48</sup> The presence of lattice fringes confirms the high crystallinity of the nanocrystals (Figure 1A,B). The silver nanodiscs exhibited an average diameter of  $38.3 \pm 9.6$  nm (see size distribution in Figure 1C), whereas

the nanoprisms showed up to double the size. The Ag nanoprisms were measured independently, and an average edge length of  $37.8 \pm 11.0$  nm was determined. The mean thickness of the nanoplates was determined as  $10.4 \pm 3.9$  nm. Figure 1D,E shows TEM micrographs of the gold nanoparticles (PhorNano HiQuant AUHQ40). The particles displayed a spherical shape with an average diameter of the AuNPs of  $38.6 \pm 7.6$  nm as determined from the TEM micrographs (Figure 1F). A very small fraction of particles with an ellipsoidal shape (as can be observed in Figure 1D) were present as well.

The light absorption properties of the synthesized nanoparticles were investigated via UV-Vis-NIR absorption spectroscopy. The normalized absorbance spectra of the aqueous dispersions of the synthesized AgNPLs and AuNPs, which were used to fabricate SERS substrates, are shown in Figure 2A. The spectra of both materials show distinct absorption peaks which can be related to the LSPR of the nanomaterials. The absorbance of the gold nanoparticles shows a relatively sharp peak centred at 530 nm with a tail extending towards higher wavelengths. Although the AuNPs still show absorption at the very frequently used Raman excitation wavelength of 785 nm, the absorbance decreases to negligibly small values towards 1000 nm. The Ag nanoplate dispersion shows a very broad LSPR absorption peak centred at a wavelength of 710 nm with a smaller shoulder at ca. 470 nm. Although the AgNPLs in aqueous dispersion show strong absorption at 785 nm, there is also still significant light absorption present at the wavelength of 1064 nm. The dashed lines in Figure 2A represent the absorbance spectra of films of the used AgNPLs and AuNPs deposited by dropcasting the dispersions on glass substrates and fully drying the resulting films. For both materials, a clear difference in comparison to

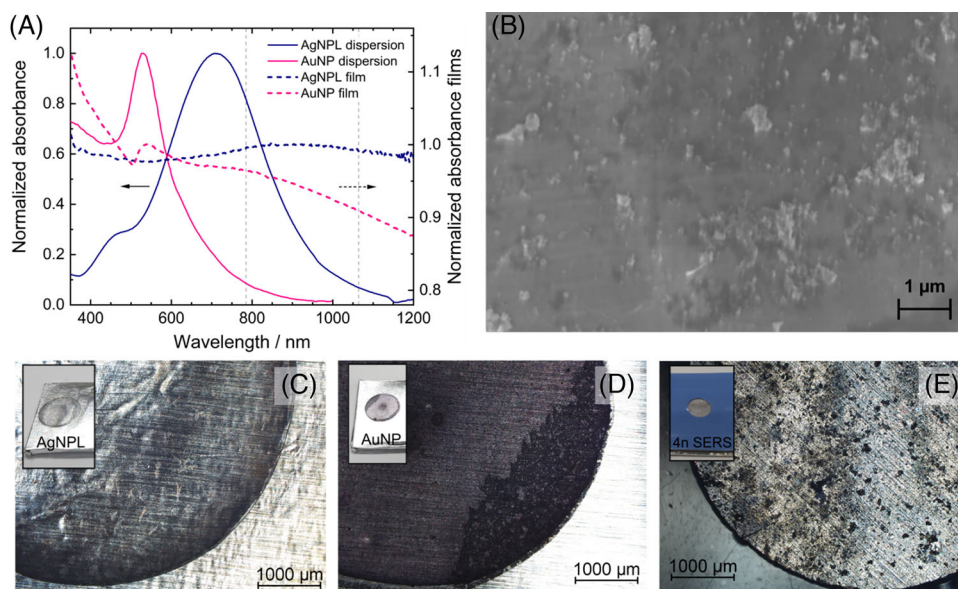


**FIGURE 2** (A) Normalized absorbance spectra of the silver nanoplates (AgNPLs) and gold nanoparticles (AuNPs) in aqueous dispersion (solid lines) and of dropcast deposited films on glass (dashed lines). The dashed grey lines are guides for the eye and indicate the wavelengths of 785 and 1064 nm. (B) Scanning electron microscopy (SEM) micrograph of a SERS substrate surface after deposition of AgNPLs on Al foil. (C–E) Micrographs of the SERS active spots of the substrates fabricated by dropcast-deposition of (C) AgNPL and (D) AuNP on aluminium foil and of (E) the commercial 4n SERS substrate. The insets show photographs of the SERS active spots on the substrates.

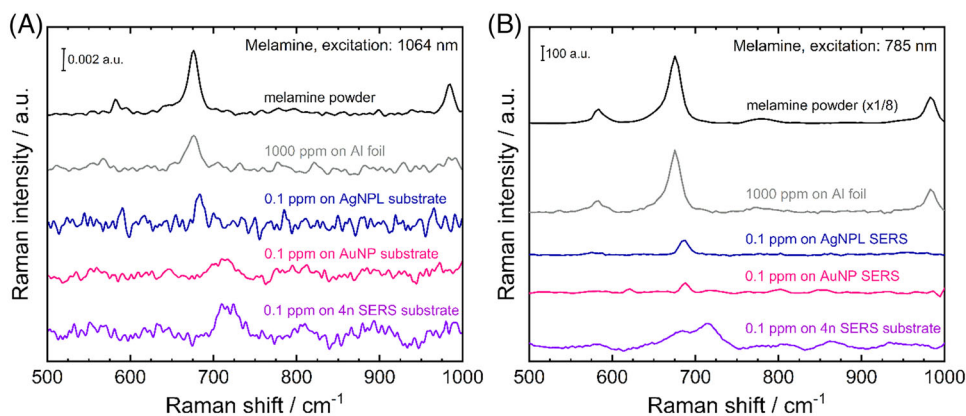
their absorbance spectra in aqueous dispersion can be observed by the strong broadening and extension of the absorption towards the NIR region. The main, well-defined LSPR absorption peaks observed in dispersion are only weakly apparent in the dropcast-deposited films. This strong shift of the light absorption may be attributed to the formation of clusters and aggregates of the Ag and Au nanomaterials during the drying of the dispersions upon dropcast deposition. Aggregation of the nanocrystals may strongly affect their plasmonic properties by inducing a shift of the spectral position of the LSPR or inducing additional higher wavelength LSPR bands.<sup>49,50</sup> Additionally, a significantly increased contribution of light scattering at the formed clusters towards the apparent absorbance must be considered for the AgNPL and AuNP film spectra. Figure 2B shows the SEM micrograph of the surface of a fabricated SERS substrate after the dropcast deposition of AgNPL on aluminium foil. The SEM image shows a distribution of small particles (<200 nm) as well as the occurrence of larger clusters/aggregates of material with sizes of several hundreds of nanometres. This observation corroborates the assumption of nanoparticle aggregation as a cause of the strong spectral shift of the absorption upon dropcast film deposition from the nanomaterial dispersions.

Figure 2C–E shows micrographs and photographs of the SERS-active spots of the investigated substrates. The substrates prepared by the dropcast-deposition of AgNPL and AuNPs show a larger amount of deposited material near the edges of the deposition area (coffee ring effect) as compared to the central area of the deposition spot, which appears to be slightly more pronounced for the AgNPL substrates. However, both types of substrates also show a homogeneous distribution of the deposited nanomaterials across the central area of

the SERS-active spot. The commercial 4n SERS substrates do not show any coffee ring pattern in the confined SERS-active spot and show a uniform and thick coverage of the Al foil support with SERS-active material.

### 3.2 | Sensitivity of SERS substrates for detection of melamine

Figure 3A,B shows the background-corrected Raman spectra measured for aqueous solutions of melamine at the indicated concentrations dropcast-deposited onto SERS substrates fabricated by the dropcast deposition of nanoparticles on Al foil as well as the commercial AuNP-based SERS substrates (4n SERS) at 1064 and 785 nm excitation, respectively. For comparison, the spectra measured for a 1000 ppm solution of melamine deposited on pristine Al foil and for melamine powder are shown. Figure 3A shows that all investigated SERS platforms can detect melamine from solutions with a very low concentration of 0.1 ppm melamine at 1064 nm excitation. This is evidenced by the occurrence of the characteristic melamine peak observed at  $684\text{ cm}^{-1}$  for AgNPL SERS and  $709\text{ cm}^{-1}$  for AuNP SERS substrates, which can be assigned to an in-plane deformation vibration of the aromatic triazine moiety.<sup>51,52</sup> A shift of the peak from the position of  $676\text{ cm}^{-1}$  measured for melamine powder and melamine on pristine Al foil can be observed for the SERS samples. Similar shifts have been frequently observed for the SERS-based detection of melamine and can be attributed to the interaction of the molecule with the metal nanostructure and/or the presence of the melamine molecules in protonated or neutral form.<sup>51,53</sup> For the AgNPL SERS substrate, the melamine peak



**FIGURE 3** (A) Background-corrected Raman spectra of melamine powder, melamine deposited from a 1000 ppm solution on Al foil and 0.1 ppm melamine solutions dropcast on the investigated SERS substrates, measured at (A) 1064 nm excitation wavelength (140 mW; 100 averaged scans) and (B) 785 nm excitation wavelength (108 mW, 32 mW for melamine powder; 1 s integration time, 10 averaged scans). The spectra were averaged over three different measurement spots on the samples. For the sake of visibility of the other spectra, the Raman intensity of the spectrum for melamine powder in (B) was divided by a factor of 8.

at a concentration of 0.1 ppm is clearly visible, whereas for the fabricated AuNP SERS substrate, the peak shows a much broader shape and a lower intensity which only barely overtops the noise level. For the commercial AuNP-based substrate (4n SERS substrate), the melamine peak shows a similar broad shape but with a significantly higher relative intensity and is clearly distinguishable from the noise level. As the LSPR of the used AuNPs does not extend to a wavelength of 1064 nm when measured in aqueous dispersion, we presume that the partial aggregation of AuNPs into larger clusters occurs during the deposition of the AuNPs, which extends the LSPR absorption bands into the NIR wavelength regime. Figure 3B shows that under excitation with a 785 nm laser, a similar detection sensitivity of 0.1 ppm melamine could be achieved for the AgNPL-based SERS substrate and the AuNP-based substrate. The peak intensities on both types of substrates are similar, with a slightly higher peak intensity observed for the AgNPL substrates. The commercial 4n SERS substrate shows a significantly higher and broader peak for a concentration of 0.1 ppm of melamine. The AEFs for the investigated SERS substrates in comparison to bare Al foil were estimated from the peak areas of the characteristic melamine peaks on Al foil (1000 ppm) and the investigated SERS substrates in Figure 3 and the corresponding melamine concentrations, according to Equation (1). The results are summarized in Table 1. All types of SERS substrates show AEFs on the order of  $10^3$ – $10^4$  for melamine in comparison to bare Al, which are comparable to literature reports.<sup>44</sup> For the comparison with support materials like glass, the additional enhancement by the Al substrate itself (AEF  $\sim$  80–240 as reported in Ref. [39]) should be considered.

It should be noted that despite the fabricated SERS substrates displaying a slightly favoured deposition of the metal nanomaterials at the edges of the SERS-active spots (coffee ring effect, see Figure 2C–D), the substrates showed good Raman signal reproducibility when measuring near the edge and across the central area of the SERS-active spot, as shown in Figure S1. Although the raw Raman spectra without background correction for AgNPL and AuNP SERS substrates

**TABLE 1** Comparison of analytical enhancement factors (AEFs) calculated for the investigated surface-enhanced Raman scattering (SERS) substrates in comparison to bare Al foil for the measurement of melamine.

Substrate	Wavelength (nm)	$C_{\text{Melamine}}$ (ppm)	Peak area (a.u.)	AEF ( $10^3$ )
Al foil	1064	1000	0.080	–
	785	1000	10,569	–
AgNPL	1064	0.1	0.051	6.4
	785	0.1	1915	1.8
AuNP	1064	0.1	0.048	4.8
	785	0.1	1210	1.1
4n SERS	1064	0.1	0.086	10.8
	785	0.1	10,157	8.9

Note: Calculations are based on Equation (1) using the peak areas of the melamine peak at  $684$ – $709$   $\text{cm}^{-1}$  determined from Figure 3.

show higher intensities of the broad background signal when measuring near the edge of the SERS-active area due to the larger amount of deposited nanomaterials, the melamine peak intensities in the background-corrected spectra show good consistency throughout the different spots. For the commercial 4n SERS substrate, the raw Raman spectra as well as the background-corrected spectra measured at different spots show little variation which can be related to a uniform layer of SERS-active metallic material across the substrate.

To assess the applicability of the fabricated AgNPL SERS substrates for the quantitative determination of analyte concentrations in comparison to the commercial 4n SERS substrates, both substrates were used for the SERS-based detection of melamine deposited from aqueous solutions of various concentrations. Figure 4 shows the averaged, background-corrected spectra for melamine deposited on AgNPL SERS substrates from solutions with melamine concentrations

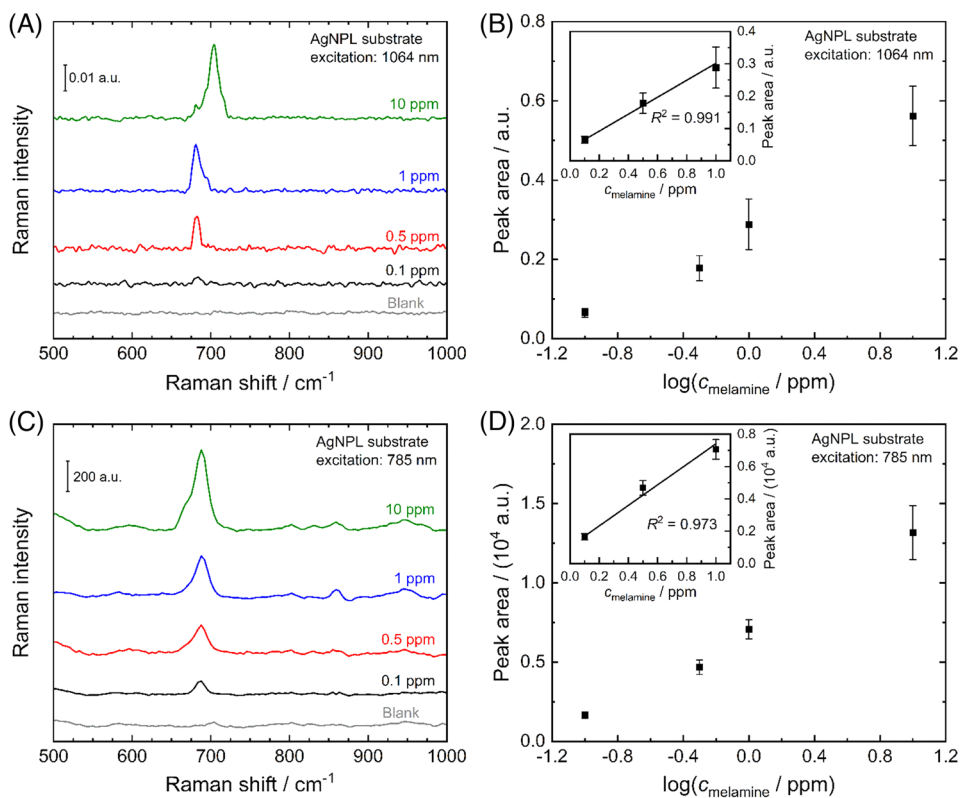


**FIGURE 4** Average background-corrected Raman spectra of a blank AgNPL SERS substrate on Al foil and of melamine deposited from solutions with concentrations ranging between 0.1 and 10 ppm onto AgNPL substrates, measured at an excitation wavelength of (A) 1064 nm (140 mW) and (C) 785 nm (108 mW). Integrated peak area of the melamine peaks centred at 687–710 cm<sup>-1</sup> plotted versus decadic logarithm of the melamine concentration  $c_{\text{melamine}}$  measured at excitation wavelengths of (B) 1064 nm and (D) 785 nm, averaged over three different spots on the samples. The insets in (B) and (D) show the peak area versus concentration curves on a linear scale for the lower melamine concentrations and the corresponding linear fit functions.

of 0.1–10 ppm measured at excitation wavelengths of 1064 nm (Figure 4A) and 785 nm (Figure 4C). From the Raman spectra measured for the different concentrations, the peak areas of the melamine peak were determined by integration for the spectra measured on three different spots on the AgNPL SERS samples. The peak areas plotted versus the decadic logarithm of the melamine concentrations ( $c_{\text{melamine}}$ ) are shown in Figure 4B (1064 nm) and Figure 4D (785 nm). The insets in Figure 4B,D show the plots of peak area versus melamine concentration on a linear scale with linear fits of the data. For both excitation wavelengths, a good linear correlation of the peak areas versus the melamine concentration on a linear scale could be observed in the lower concentration regime (0.1–1 ppm melamine) as shown by coefficients of determination ( $R^2$ ) close to 1.

The averaged, background-corrected Raman spectra for melamine solutions with different concentrations deposited on 4n SERS substrates are shown in Figure 5A for 1064 nm and Figure 5C for 785 nm, respectively. The corresponding peak area versus logarithmic concentration diagrams are shown in Figure 5B (1064 nm) and Figure 5D (785 nm). The insets of the graphs show the peak area versus linear melamine concentration in the lower concentration range. For both Raman excitation wavelengths, the peak areas showed an excellent linear correlation with the melamine concentration in the lower con-

centration range for the 4n SERS substrate. The relatively small error bars indicate the good spot-to-spot reproducibility of the SERS signal on the 4n SERS substrate. The linear fit functions of peak area versus melamine concentration and the peak areas determined from the replicates of the blank SERS substrate measurements in the same wavenumber range were used to calculate the LOD for the detection of melamine on AgNPL-based and commercial 4n SERS substrates, as described in Section 2.4. The determined LOD values are summarized in Table 2. At an excitation wavelength of 1064 nm, both the AgNPL-based substrate and the 4n SERS substrate show similar LOD of 63 and 66 ppb for melamine, respectively. At 785 nm Raman excitation, the performance of the commercial 4n substrate surpasses the AgNPL SERS substrate with an LOD of 8 ppb in comparison to 34 ppb for the AgNPL substrate. These values for the LOD for melamine are comparable to those reported by Gudun et al. (27 ppb) for AuNP–Al foil-based substrates<sup>40</sup> and the melamine LOD reported for expensive, high-performance Klarite SERS substrates (33 ppb) reported by Lin et al.<sup>54</sup> for excitation at 785 nm.

The results indicate that the fabricated AgNPL SERS substrate shows a good applicability for quantitative melamine detection similar to the performance of commercial AuNP-based 4n SERS substrates. The 4n SERS substrates showed slight superiority in terms of detection

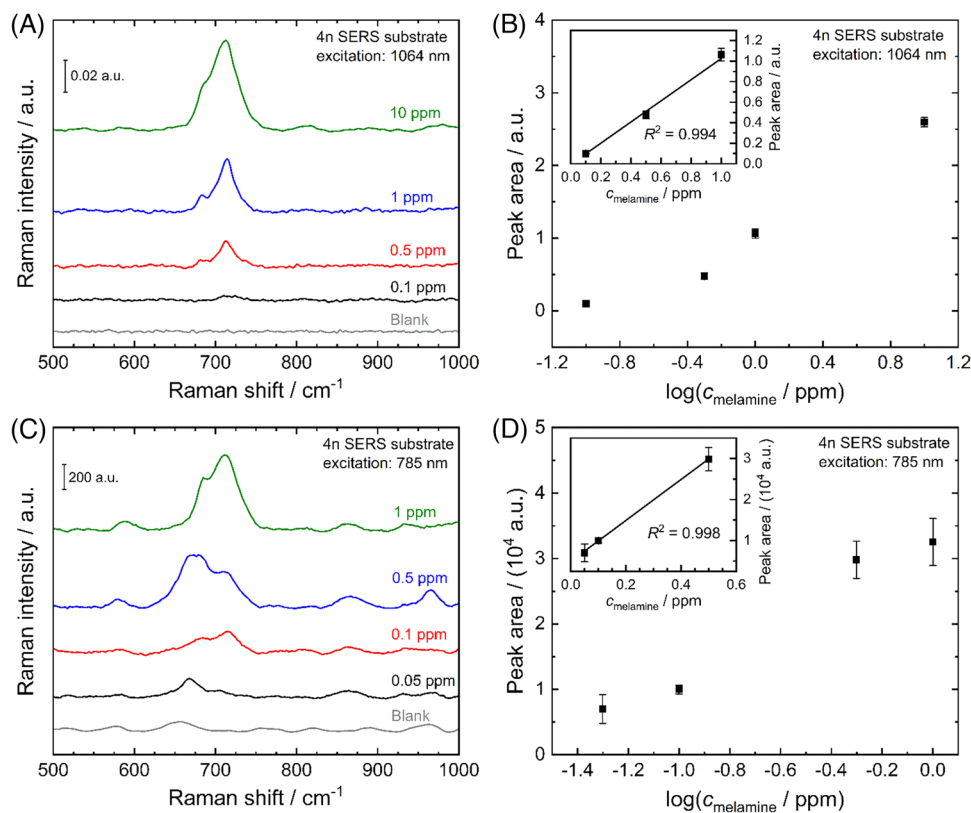


**FIGURE 5** Average background-corrected Raman spectra of the blank 4n SERS substrate and of melamine deposited from solutions with concentrations ranging between 0.05 and 10 ppm onto the 4n SERS substrates, measured at an excitation wavelength of (A) 1064 nm (140 mW) and (C) 785 nm (108 mW). Integrated peak area of the melamine peaks centred at 687–710 cm<sup>-1</sup> plotted versus decadic logarithm of the melamine concentration  $c_{\text{melamine}}$  measured at excitation wavelengths of (B) 1064 nm and (D) 785 nm, averaged over three different spots on the samples. The insets in (B) and (D) show the peak area versus concentration curves on a linear scale for the lower melamine concentrations and the corresponding linear fit functions.

**TABLE 2** Limit of detection (LOD) values (in parts per billion, ppb) calculated for the AgNPL-based surface-enhanced Raman scattering (SERS) substrates and the commercial 4n SERS substrates as outlined in Section 2.4.

Substrate	Wavelength (nm)	$k_{\text{Fit}}$ (a.u. ppm <sup>-1</sup> )	$d_{\text{Fit}}$ (a.u.)	$\bar{I}_{\text{Blank}}$ (a.u.)	$s_{\text{Blank}}$ (a.u.)	LOD (ppb)
AgNPL	1064	0.262	0.039	0.036	0.0065	63
	785	6342	1061	708	190	34
4n SERS	1064	1.032	-0.0054	0.042	0.0069	66
	785	49,950	4927	3404	637	8

Note:  $k_{\text{Fit}}$  and  $d_{\text{Fit}}$  are the slope and intercept of the linear fit function of the peak area versus melamine concentration graphs measured for the substrates (see Figures 4 and 5).  $\bar{I}_{\text{Blank}}$  is the mean peak area determined from Raman measurements on the blank SERS substrates, and  $s_{\text{Blank}}$  is the standard deviation of the peak area values for the blank replicate measurements.

sensitivity at 785 nm excitation and spot-to-spot reproducibility of the Raman signal.

### 3.3 | Damage threshold and storage stability of fabricated SERS substrates

To assess the maximum laser power which the fabricated AgNPL-based Al foil SERS substrates can sustain in comparison to the commercial

4n SERS substrates, measurements with a successive increase of excitation laser power on the same measurement spot were performed for both substrates. Melamine, which was dropcast-deposited onto the substrates from solutions of 0.1 or 1 ppm, was used as a test analyte to assess if laser-induced damage of the SERS substrate occurred as indicated by a non-uniform increase or decrease of the measured SERS signal above the damage threshold laser power. The background-corrected Raman spectra measured for AgNPL-based substrates and 4n SERS substrates at different laser powers at 1064 and 785 nm are



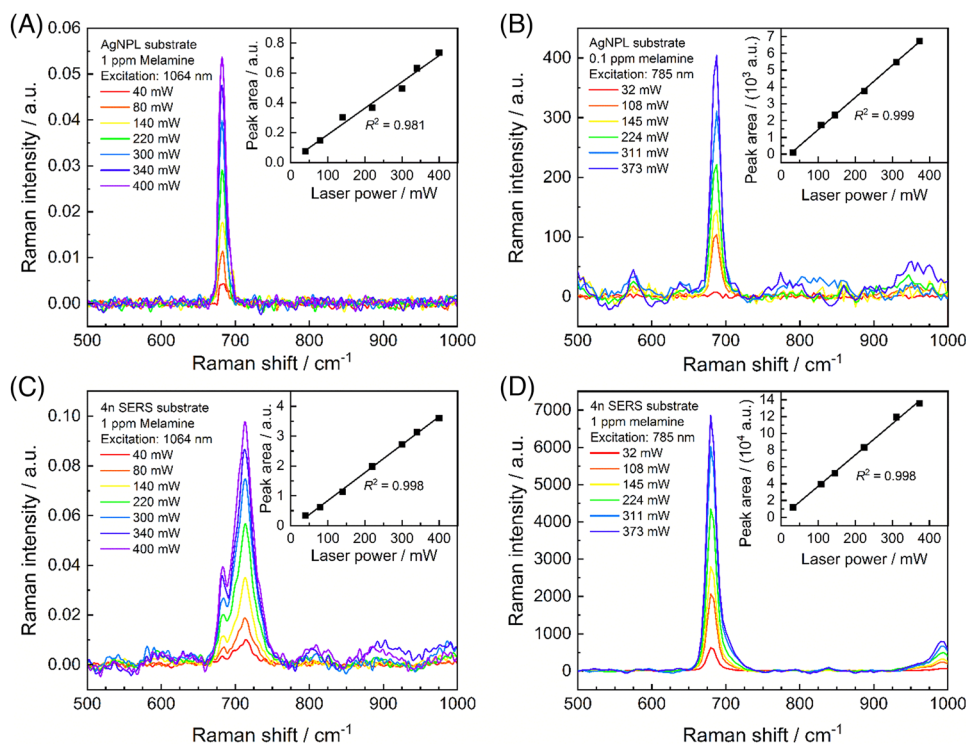


**FIGURE 6** Background-corrected Raman spectra of 0.1 and 1 ppm melamine solutions dropcast-deposited on (A and B) AgNPL-based SERS substrates and (C and D) 4n SERS substrates, respectively, measured at increasing laser power at 1064 nm (A and C) and 785 nm (B and D) on the same measurement spot. The insets show the integrated peak area of the characteristic melamine peak versus the excitation laser power fitted with a linear function.

shown in Figure 6. In Figure 6C, a slight shift of the melamine peak position in comparison to the other spectra can be observed, which may be attributed to a difference due to the local presence of melamine in protonated or neutral form<sup>51,52</sup> or interaction with residual traces of water. The insets of the graphs in Figure 6 show the corresponding integrated peak area of the melamine peak at 687–710  $\text{cm}^{-1}$  plotted versus the excitation laser power. As evident from the insets, both SERS platforms showed no deviation from the expected linear increase of signal intensity with laser power over the whole available power ranges of up to 400 mW at 1064 nm and 373 mW at 785 nm, respectively. We attribute this extraordinarily high damage threshold and signal stability to a heat sink effect of the Al foil substrate, enhanced by the thin layer of noble metal nanoparticles, which allows the rapid dissipation of the heat generated by laser absorption. This may effectively prevent local thermal damage of the SERS substrate and the analyte molecules and allows to perform Raman analysis with high laser powers, which strongly benefits the obtainable analyte sensitivity.

In addition to the laser damage threshold, the ambient storage stability of the investigated substrates was tested by the measurement of melamine on SERS substrates after different periods of storage under ambient conditions (see Figure S2). All three substrates showed a good reproducibility of the Raman signal measured on substrates after 14 days of ambient ageing in comparison to freshly prepared substrates. After a total of 40 days of storage under ambient conditions, the AgNPL substrates showed a loss of the enhancement effect, whereas

the AuNP-based substrates could still detect the same concentration of melamine albeit with a clearly decreased signal intensity. The commercial SERS substrates showed very good ambient storage stability with the signal enhancement persisting for more than 280 days of storage.

### 3.4 | Sensitivity of SERS substrates for rhodamine 6G detection

To check the performance of the investigated SERS substrates for the detection of analytes other than melamine, Raman measurements on the substrates after deposition of the dye R6G from solutions in water were carried out. The background-corrected Raman spectra for the lowest R6G concentrations which were still detectable with the investigated SERS substrates are shown in Figure 7. For comparison, the spectra of pristine R6G powder and of R6G deposited on plain aluminium foil from a 1000 ppm solution are shown. For the AgNPL-based SERS substrate, a clear detection of the three main Raman peaks of R6G at wavenumbers of 1309, 1362 and 1510  $\text{cm}^{-1}$  could be observed at concentrations as low as 0.1 ppm. For the commercial 4n SERS substrate, the detection of the R6G peaks could similarly be achieved down to concentrations of 0.1 ppm albeit with a slightly lower signal intensity relative to the noise level. The AgNPL-based substrate and the 4n SERS substrate thus show comparable performance in the detection of R6G and melamine. The fabricated AuNP SERS substrate shows a worse

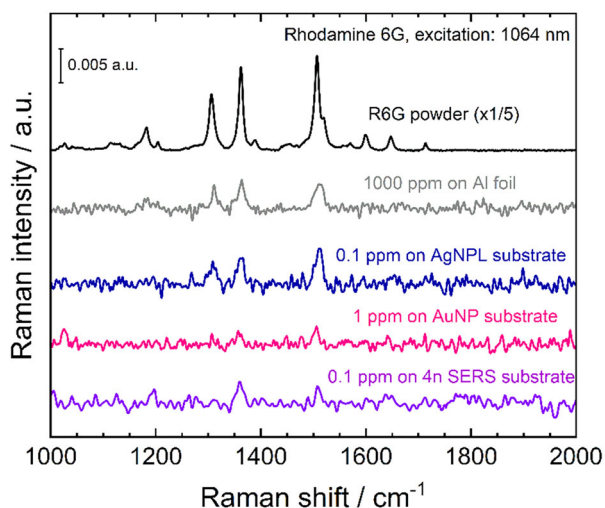


**FIGURE 7** Background-corrected Raman spectra of rhodamine 6G (R6G) powder, R6G deposited from a 1000 ppm solution on Al foil and 0.1 or 1 ppm R6G solutions dropcast on the investigated SERS substrates, measured at 1064 nm excitation wavelength (140 mW, 100 averaged scans). The spectra were averaged over three different measurement spots on the samples. For the sake of visibility, the Raman intensity of the spectrum for R6G powder was divided by a factor of 5.

**TABLE 3** Comparison of analytical enhancement factors (AEF) calculated for the surface-enhanced Raman scattering (SERS) substrates in comparison to bare Al foil for the measurement of rhodamine 6G at 1064 nm excitation.

Substrate	Wavelength (nm)	$c_{\text{R6G}}$ (ppm)	Peak area (a.u.)	AEF ( $10^3$ )
Al foil	1064	1000	0.087	–
AgNPL	1064	0.1	0.096	11.1
AuNP	1064	1	0.039	0.4
4n SERS	1064	0.1	0.040	4.6

Note: Calculations are based on Equation (1), using the peak areas of the R6G peak at  $1510\text{ cm}^{-1}$  (Figure 7).

performance for the measurement of R6G where the detection of the characteristic peaks could be achieved only at 1 ppm or above. From the peak areas of the R6G peak at  $1510\text{ cm}^{-1}$ , the AEFs for the different types of SERS substrates compared to bare aluminium foil were estimated via Equation (1). The resulting AEFs are listed in Table 3. In comparison to melamine, AEFs of similar magnitude are found for the AgNPL SERS substrates and the commercial 4n SERS, whereas the fabricated AuNP SERS substrates show a significantly lower AEF.

## 4 | CONCLUSIONS

In this work, we demonstrated the fabrication of SERS substrates based on a simple dropcast deposition method of Ag nanoplates and spherical Au nanoparticles on untreated aluminium foil. Due to the

choice of the used nanomaterials and a shift of their light absorption properties towards the NIR upon dropcast deposition, we achieve an excellent sensitivity of the substrates for the use with the NIR excitation wavelength of 1064 nm. The fabricated SERS substrates show a good performance for the trace detection of melamine and R6G at concentrations of 0.1 ppm and below, with AEFs of up to  $10^4$  in comparison to bare aluminium foil. Furthermore, we demonstrated the extraordinarily high laser excitation power tolerance of the fabricated substrates, which showed excellent stabilities of the measured analyte signals at excitation power of up to 373 mW at 785 nm and 400 mW at 1064 nm. The simple fabrication, robustness and great suitability for NIR excitation make the demonstrated SERS substrates excellent candidates for cost-effective chemical sensing applications, especially for analytes which show photoinstability and/or fluorescence in the visible wavelength range.

## ACKNOWLEDGEMENTS

The authors gratefully acknowledge financial support from the Austrian Research Promotion Agency (FFG) within the program Beyond Europe (Project: MODERNA, No. 874147). Felix Mayr gratefully acknowledges financial support from the Austrian Research Promotion Agency (FFG) within the program e!MISSION Austria (Project Plas-Ion-PhotoKat, Grant No. 888408). The authors gratefully acknowledge support by the Johannes Kepler Open Access Publishing Fund of the Johannes Kepler University Linz. The authors gratefully acknowledge the technical support by Peter Oberhumer (ZONA, Johannes Kepler University Linz) for the TEM measurements.

## CONFLICT OF INTEREST STATEMENT

There are no conflicts of interest to declare.

## DATA AVAILABILITY STATEMENT

The data that support the findings of this study are available from the corresponding author upon request.

## ORCID

Felix Mayr  <https://orcid.org/0000-0003-2414-233X>

Robert Zimmerleiter  <https://orcid.org/0000-0001-9933-0330>

Mateusz Bednorz  <https://orcid.org/0000-0002-9160-3338>

Yolanda Salinas  <https://orcid.org/0000-0002-1828-5839>

André Galembeck  <https://orcid.org/0000-0002-6361-9869>

Dominik Wielend  <https://orcid.org/0000-0003-1330-9915>

Tania M. Brito-Silva  <https://orcid.org/0009-0004-0606-2146>

Eduardo Padrón-Hernández  <https://orcid.org/0000-0002-1492-1199>

Peter Burgholzer  <https://orcid.org/0000-0003-3383-803X>

Markus C. Scharber  <https://orcid.org/0000-0002-4918-4803>

Niyazi Serdar Sariciftci  <https://orcid.org/0000-0003-4727-1193>

## REFERENCES

- Hertz H. Ueber einen Einfluss des ultravioletten Lichtes auf die elektrische Entladung. *Ann Phys.* 1887;267(8):983-1000. doi:10.1002/andp.18872670827

2. Jho H, Lee B, Ji Y, Ha S. Discussion for the enhanced understanding of the photoelectric effect. *Eur J Phys*. 2023;44:025301. doi:10.1088/1361-6404/acb39d
3. Maier SA, Atwater HA. Plasmonics: localization and guiding of electromagnetic energy in metal/dielectric structures. *J Appl Phys*. 2005;98:011101. doi:10.1063/1.1951057
4. Mayer KM, Hafner JH. Localized surface plasmon resonance sensors. *Chem Rev*. 2011;111:3828-3857. doi:10.1021/cr100313v
5. Willets KA, Van Duyne RP. Localized surface plasmon resonance spectroscopy and sensing. *Annu Rev Phys Chem*. 2007;58:267-297. doi:10.1146/annurev.physchem.58.032806.104607
6. Petryayeva E, Krull UJ. Localized surface plasmon resonance: nanostructures, bioassays and biosensing—a review. *Anal Chim Acta*. 2011;706:8-24. doi:10.1016/j.aca.2011.08.020
7. Kovacs GJ, Loutfy RO, Vincett PS. Distance dependence of SERS enhancement factor from Langmuir-Blodgett monolayers on metal island films: evidence for the electromagnetic mechanism. *Langmuir*. 1986;2(6):689-694. doi:10.1021/la00072a001
8. Li C, Huang Y, Li X, et al. Towards practical and sustainable SERS: a review of recent developments in the construction of multifunctional enhancing substrates. *J Mater Chem C*. 2021;9:11517-11552. doi:10.1039/d1tc02134f
9. Moskovits M. Surface-enhanced Raman spectroscopy: a brief retrospective. *J Raman Spectrosc*. 2005;36:485-496. doi:10.1002/jrs.1362
10. Le Ru EC, Blackie E, Meyer M, Etchegoin PG. Surface enhanced Raman scattering enhancement factors: a comprehensive study. *J Phys Chem C*. 2007;111:13794-13803. doi:10.1021/jp0687908
11. Huang Y, Liu W, Gong Z, et al. Detection of buried explosives using a surface-enhanced Raman scattering (SERS) substrate tailored for miniaturized spectrometers. *ACS Sens*. 2020;5:2933-2939. doi:10.1021/acssensors.0c01412
12. Chou A, Jaatinen E, Buividas R, et al. SERS substrate for detection of explosives. *Nanoscale*. 2012;4:7419-7424. doi:10.1039/C2NR32409A
13. Wu J, Zhang L, Huang F, Ji X, Dai H, Wu W. Surface enhanced Raman scattering substrate for the detection of explosives: construction strategy and dimensional effect. *J Hazard Mater*. 2020;387:121714. doi:10.1016/j.jhazmat.2019.121714
14. Tang X, Dong R, Yang L, Liu J. Fabrication of Au nanorod-coated Fe<sub>3</sub>O<sub>4</sub> microspheres as SERS substrate for pesticide analysis by near-infrared excitation. *J Raman Spectrosc*. 2015;46:470-475. doi:10.1002/jrs.4658
15. Pang S, Yang T, He L. Review of surface enhanced Raman spectroscopy (SERS) detection of synthetic chemical pesticides. *TrAC Trends Anal Chem*. 2016;85:73-82. doi:10.1016/j.trac.2016.06.017
16. Jiao S, Liu Y, Wang S, et al. Face-to-face assembly of Ag nanoplates on filter paper for pesticide detection by surface-enhanced Raman spectroscopy. *Nanomaterials*. 2022;12:1398. doi:10.3390/nano12091398
17. Alula MT, Mengesha ZT, Mwenesongole E. Advances in surface-enhanced Raman spectroscopy for analysis of pharmaceuticals: a review. *Vib Spectrosc*. 2018;98:50-63. doi:10.1016/j.vibspec.2018.06.013
18. Alharbi O, Xu Y, Goodacre R. Detection and quantification of the opioid tramadol in urine using surface enhanced Raman scattering. *Analyst*. 2015;140:5965-5970. doi:10.1039/c5an01177a
19. Cialla D, Pollok S, Steinbrücker C, Weber K, Popp J. SERS-based detection of biomolecules. *Nanophotonics*. 2014;3(6):383-411. doi:10.1515/nanoph-2013-0024
20. Shaine ML, Premasiri WR, Ingraham HM, et al. Surface enhanced Raman scattering for robust sensitive detection and confirmatory identification of dried bloodstains. *Analyst*. 2020;145:6097-6110. doi:10.1039/d0an01132k
21. Fazio B, D'Andrea C, Foti A, et al. SERS detection of biomolecules at physiological pH via aggregation of gold nanorods mediated by optical forces and plasmonic heating. *Sci Rep*. 2016;6:26952. doi:10.1038/srep26952
22. Guo Y, Girmatsion M, Li H-W, et al. Rapid and ultrasensitive detection of food contaminants using surface-enhanced Raman spectroscopy-based methods. *Crit Rev Food Sci Nutr*. 2021;61:3555-3568. doi:10.1080/10408398.2020.1803197
23. Mosier-Boss PA. Review of SERS substrates for chemical sensing. *Nanomaterials*. 2017;7:142. doi:10.3390/nano7060142
24. Choi J, Kim J-H, Oh J-W, Nam J-M. Surface-enhanced Raman scattering-based detection of hazardous chemicals in various phases and matrices with plasmonic nanostructures. *Nanoscale*. 2019;11:20379-20391. doi:10.1039/c9nr07439b
25. Lai C-H, Wang G-A, Ling T-K, et al. Near infrared surface-enhanced Raman scattering based on star-shaped gold/silver nanoparticles and hyperbolic metamaterial. *Sci Rep*. 2017;7:5446. doi:10.1038/s41598-017-05939-0
26. Sosa IO, Noguez C, Barrera RG. Optical properties of metal nanoparticles with arbitrary shapes. *J Phys Chem B*. 2003;107:6269-6275. doi:10.1021/jp0274076
27. Noguez C. Surface plasmons on metal nanoparticles: the influence of shape and physical environment. *J Phys Chem C*. 2007;111:3806-3819. doi:10.1021/jp066539m
28. Chen C-F, Tzeng S-D, Chen H-Y, Lin K-J, Gwo S. Tunable plasmonic response from alkanethiolate-stabilized gold nanoparticle superlattices: evidence of near-field coupling. *J Am Chem Soc*. 2008;130:824-826. doi:10.1021/ja0773610
29. Garg V, Sengar BS, Awasthi V, et al. Localized surface plasmon resonance on Au nanoparticles: tuning and exploitation for performance enhancement in ultrathin photovoltaics. *RSC Adv*. 2016;6:26216-26226. doi:10.1039/c5ra25575a
30. Blaber MG, Schatz GC. Extending SERS into the infrared with gold nanosphere dimers. *Chem Commun*. 2011;47:3769-3771. doi:10.1039/c0cc05089j
31. Greeneltch NG, Davis AS, Valley NA, et al. Near-infrared surface-enhanced Raman spectroscopy (NIR-SERS) for the identification of Eosin Y: theoretical calculations and evaluation of two different nanoplasmonic substrates. *J Phys Chem A*. 2012;116:11863-11869. doi:10.1021/jp3081035
32. Skrabic M, Kosovic M, Gotic M, Mikac L, Ivanda M, Gamulin O. Near-infrared surface-enhanced Raman scattering on silver-coated porous silicon photonic crystals. *Nanomaterials*. 2019;9:421. doi:10.3390/nano9030421
33. Kearns H, Ali F, Bedics MA, et al. Sensitive SERS nanotags for use with a hand-held 1064 nm Raman spectrometer. *R Soc Open Sci*. 2017;4:170422. doi:10.1098/rsos.170422
34. Lynn KA, McNay G, Eustace DA, Shand NC, Smith WE. Short-wave infrared excited SERS. *Analyst*. 2010;135:1904-1905. doi:10.1039/C0AN00096E
35. Kneipp K, Roth E, Engert C, Kiefer W. Near-infrared surface-enhanced Raman spectroscopy of rhodamine 6G on colloidal silver. *Chem Phys Lett*. 1993;207:450-454. doi:10.1016/0009-2614(93)89028-G
36. Meyer MW, Smith EA. Optimization of silver nanoparticles for surface enhanced Raman spectroscopy of structurally diverse analytes using visible and near-infrared excitation. *Analyst*. 2011;136:3542-3549. doi:10.1039/c0an00851f
37. McLintock A, Cunha-Matos CA, Zagnoni M, Millington OR, Wark AW. Universal surface-enhanced Raman tags: individual nanorods for measurements from the visible to the infrared (514-1064 nm). *ACS Nano*. 2014;8(8):8600-8609. doi:10.1021/nn503311d
38. Kearns H, Shand NC, Smith WE, Faulds K, Graham D. 1064 nm SERS of NIR active hollow gold nanotags. *Phys Chem Chem Phys*. 2015;17:1980-1986. doi:10.1039/c4cp04281f
39. Betz JF, Yu WW, Cheng Y, White IM, Rubloff GW. Simple SERS substrates: powerful, portable, and full of potential. *Phys Chem Chem Phys*. 2014;16:2224-2239. doi:10.1039/c3cp53560f
40. Gudun K, Elemessova Z, Khamkhash L, Ralchenko E, Bukasov R. Commercial gold nanoparticles on untreated aluminum foil: versatile,

- sensitive, and cost-effective SERS substrate. *J Nanomater.* 2017;2017:9182025. doi:10.1155/2017/9182025
41. Martinez-Garcia MM, Cardoso-Avila PE, Pichardo-Molina JL. Concave gold nanocubes on Al-6063 alloy as a simple and efficient SERS substrate. *Colloids Surf A.* 2016;493:66-73. doi:10.1016/j.colsurfa.2016.01.030
42. Woodcraft AL. Recommended values for the thermal conductivity of aluminium of different purities in the cryogenic to room temperature range, and a comparison with copper. *Cryogenics.* 2005;45:626-636. doi:10.1016/j.cryogenics.2005.06.008
43. Mogensen KB, Gühlke M, Kneipp J, et al. Surface-enhanced Raman scattering on aluminum using near infrared and visible excitation. *Chem Commun.* 2014;50:3744-3746. doi:10.1039/c4cc00010b
44. Lopez MI, Ruisanchez I, Callao MP. Figures of merit of a SERS method for Sudan I determination at trace levels. *Spectrochim Acta Part A.* 2013;111:237-241. doi:10.1016/j.saa.2013.04.031
45. Ceballos M, Arizmendi-Morquecho A, Sanchez-Dominguez M, Lopez I. Electrochemical growth of silver nanodendrites on aluminum and their application as surface-enhanced Raman spectroscopy (SERS) substrates. *Mater Chem Phys.* 2020;240:122225. doi:10.1016/j.matchemphys.2019.122225
46. Sharma K, Paradakar M. The melamine adulteration scandal. *Food Sec.* 2010;2:97-107. doi:10.1007/s12571-009-0048-5
47. Zhang Q, Li N, Goebel J, Lu Z, Yin Y. A systematic study of the synthesis of silver nanoplates: is citrate a "Magic" reagent? *J Am Chem Soc.* 2011;133:18931-18939. doi:10.1021/ja2080345
48. Zhang Q, Hu Y, Guo S, Goebel J, Yin Y. Seeded growth of uniform Ag nanoplates with high aspect ratio and widely tunable surface plasmon bands. *Nano Lett.* 2010;10:5037-5042. doi:10.1021/nl1032233
49. Westcott SL, Oldenburg SJ, Lee TR, Halas NJ. Construction of simple gold nanoparticle aggregates with controlled plasmon-plasmon interactions. *Chem Phys Lett.* 1999;300:651-655. doi:10.1016/S0009-2614(98)01410-9
50. Lee J, Lee K, Lim CT. Surface plasmon resonance assay for identification of small molecules capable of inhibiting A $\beta$  aggregation. *ACS Appl Mater Interfaces.* 2021;13:27845-27855. doi:10.1021/acsami.1c04833
51. Wang R, Xu Y, Wang R, et al. A microfluidic chip based on an ITO support modified with Ag-Au nanocomposites for SERS based determination of melamine. *Microchim Acta.* 2017;184:279-287. doi:10.1007/s00604-016-1990-5
52. Rajapandiyar P, Tang W-L, Yang J. Rapid detection of melamine in milk liquid and powder by surface-enhanced Raman scattering substrate array. *Food Control.* 2015;56:155-160. doi:10.1016/j.foodcont.2015.03.028
53. Mircescu NE, Oltean M, Chis V, Leopold N. FTIR, FT-Raman, SERS and DFT study on melamine. *Vib Spectrosc.* 2012;62:165-171. doi:10.1016/j.vibspec.2012.04.008
54. Lin M, He L, Awika J, et al. Detection of melamine in gluten, chicken feed, and processed foods using surface enhanced Raman spectroscopy and HPLC. *J Food Sci.* 2008;73(8):129-134. doi:10.1111/j.1750-3841.2008.00901.x

### SUPPORTING INFORMATION

Additional supporting information can be found online in the Supporting Information section at the end of this article.

**How to cite this article:** Mayr F, Zimmerleiter R, Farias PMA, et al. Sensitive and high laser damage threshold substrates for surface-enhanced Raman scattering based on gold and silver nanoparticles. *Anal Sci Adv.* 2023;4:335-346.  
<https://doi.org/10.1002/ansa.202300033>